Nanostructured ZnO Interphase for Carbon Fiber Reinforced Composites with Strain Rate Tailored Interfacial Strength

Jalal Nasser, Kelsey Steinke, Hyun-Sik Hwang, and Henry Sodano*

Composite materials designed for ballistic applications typically require fiber–matrix interfacial properties which are considerably different than those used in more common structural applications. Ballistic composites are usually benefited through the use of a weaker interface that allows the high tenacity of the fiber to be utilized for energy absorption, whereas structural composites require strong interfaces to ensure materials which do not easily delaminate or experience cracking. Here, the multifunctionality of a zinc oxide (ZnO) interphase through a tailored interfacial shear strength (IFSS) as a function of strain rate is demonstrated. Both ZnO nanowires (NWs) and nanoparticles (NPs) are shown through variable strain rate pullout to enable tailored behavior with the NWs producing an 87% increase in IFSS over untreated fibers under quasi-static loading, and 53% lower interfacial shear strength than untreated fibers at 2200 s^{-1}. The reduced interfacial strength under dynamic loading conditions is attributed to the polymer's viscoelasticity, as matrix stiffening effects reduce the NWs' functional gradient, causing brittle failure of the ceramic interphase. The results demonstrate the potential for ZnO NWs and NPs to enable the tailored design of interfaces and to realize multifunctional materials with optimal behavior under both static and dynamic loading conditions.

1. Introduction

Multifunctional materials are designed such that they combine two or more functions that are typically accomplished using separate materials or systems into a single material. The most common structural multifunctional materials over the past decade have focused on incorporating self-healing,[1–4] energy harvesting,[5–8] sensing,[9–11] and health monitoring[12–15] into the structure. For example, the integration of nanoscale piezoelectric materials in continuous fiber reinforced polymer composites have allowed for structural components to harness wasted kinetic energy from mechanical vibrations in aerospace and automotive applications. This leads to a reduction in the weight and complexity of these structures through partially or completely eliminating additional components, such as of batteries, where the structure itself is able to contribute toward meeting the system's energy requirements.[6] However, multifunctional materials can also be of great use in less obvious applications. For instance, ballistic materials are often designed separately from the structure and serve the sole purpose of providing protection from high energy impacts and blasts.[16] Currently, ballistic protection for ground vehicles and stationary shelters comes in the form of heavy and expensive add-on armor.[17] Moreover, in the case of ground vehicles, such armor considerably reduces maneuverability and fuel efficiency, two critical factors for their performance when operating during combat.[16] Given that the armor is a combination of metallic, ceramic, and composite materials, merging and bonding them together into one part in a proper, efficient, and cost-effective manner remains a challenging production task. Therefore, a need exists for a single multifunctional material that combines both high ballistic and structural performances, while satisfying flexibility, weight, and cost requirements.

Numerous techniques and methods have emerged to produce multifunctional systems with simultaneous high ballistic and structural performances. In the mid-nineties, Fink et al. presented a multi-layer structural laminate for ground combat vehicle protection.[18,19] The proposed composite integral armor (CIA) included ceramic alumina tiles for ballistic protection and a thick section composite plate to act as structural backing. However, the CIA possessed a low mass efficiency that fell considerably short from satisfying weight requirements of military applications. Other methods aim to reduce the system's weight through the use of polymer fiber reinforced polymer matrix composite laminates for ballistic reinforcement. This is evident in the design of U.S. military helmets, where carbon fiber shells are over-molded with layers of high-molecular-weight polypropylene in order to simultaneously provide structural integrity and ballistic protection.[20–22] Alternatively, Harach et al.

J. Nasser, Prof. H. Sodano
Department of Aerospace Engineering
University of Michigan
Ann Arbor, MI 48109, USA
E-mail: hsodano@umich.edu
K. Steinke, Prof. H. Sodano
Department of Materials Science and Engineering
University of Michigan
Ann Arbor, MI 48109, USA
Dr. H.-S. Hwang
Samsung Electronics
Maetan-dong, Suwon-Si 443-743, South Korea

The ORCID identification number(s) for the author(s) of this article can be found under https://doi.org/10.1002/admi.201901544.

**ADVANCED
SCIENCE NEWS**
www.advancedsciencenews.com

**ADVANCED
MATERIALS
INTERFACES**
www.advmatinterfaces.de

developed metallic–intermetallic laminates (MIL) as a new class of synthetic multifunctional materials.[23] Inspired by the multifunctionality of biological systems, titanium and aluminum foils are processed to produce metallic laminates with hierarchal microstructures that allow for good structural and ballistic performance, among their other unique properties. While such composites achieve multifunctionality without the need for multiple components, the high areal density and rigidity of MIL limited its use in applications where flexibility and light-weight are of high importance.[24] Another approach to introduce multifunctionality into fiber reinforced composites in the form of ballistic protection is through modifying the choice of the matrix resin. Vieille et al.[25] conducted a comparative study on thermoplastic and thermosetting-based carbon fiber laminates and found that the former exhibited smaller delamination and better blast impact performance. Yet weak fiber–matrix interfaces and low melting points have restricted thermoplastic resins to consumer applications. Recently, considerable interest has been shown in introducing multifunctionality into carbon and glass fiber reinforced polymer matrix composites for a high structural and ballistic performance using various techniques.[26–28] Carbon and glass fibers reinforced composites possess properties such as high tensile strength, high stiffness, and considerably low strain to failure, making them suitable for structural applications, but not ideal for most ballistic ones.[29] This is primarily due to the localization of failure at the point of impact when these composites are struck by a projectile.[30] One way to integrate multifunctionality into these composites is through the design of a fiber–matrix interface that maximizes structural performance at low strain rate loading conditions, while improving its energy absorption at high strain rates. A weaker interface would enable the tough fiber to absorb impact energy, whereas a strong interface would increase a composite's resistance to delamination and matrix cracking under static loading. Such multifunctionality would eliminate the need for multi-components protection systems, while satisfying weight, flexibility, and cost requirements. Many sizing techniques,[31–33] and chemical and plasma treatments[33,34] have been reported on carbon and glass fibers with the goal of tailoring the fiber–matrix interface for multifunctionality. However, most of these methods end up damaging the fibers' core and etching its surface, leading to a considerable reduction in the fiber's tensile strength, and thus sacrificing its structural performance for an improvement in its ballistic properties.

An alternative approach for modifying the fiber–matrix interface of carbon fiber reinforced polymer composites to achieve the desired multifunctionality is through interphase design. The introduction of nanomaterials on the fiber's surface creates a hierarchical interface between the interfacial components which provides the composite with unique characteristics. This nanostructured interphase is usually achieved through grafting or whiskerization methods. For instance, grafting of carbon nanotubes (CNTs) onto the carbon fibers surfaces has garnered significant interest in recent years due to their excellent mechanical properties, as well as their ability to draw thermal energy from the matrix to the fibers.[35–38] At static loading conditions, Downs and Bakera[39] showed an increase in the interfacial shear strength (IFSS) of more than 400% in carbon fiber composites with a hierarchical CNT interphase. However,

similar measurements of single carbon fiber composites IFSS under dynamic loading conditions are unavailable in literature due to the difficulty of replicating the necessary experimental conditions using dynamic actuators. This has led to greater focus on studying the bulk properties of CNT reinforced carbon fiber reinforced composites when dynamically loaded. Sharma and Lakkad[35] reported 48% increase in impact strength in CNTs-coated carbon fiber reinforced composites when tested using a drop tower impact system. The improvement in impact strength is attributed to the ability of CNTs to bridge micro-cracks near the fiber matrix. However, CNTs' synthesis is performed by high temperature chemical vapor deposition processes using catalysts which react with the carbon fiber, resulting in significant degradation of the fiber strength. Thus, the interfacial improvement gained under static and dynamic loading conditions comes at the expense of reduced in-plane properties of the composite. The excellent mechanical properties of CNTs also make them well suited for use as a reinforcement in nanocomposites inside the resin of carbon fiber laminated structures used in ballistic applications. However, the use of a CNT reinforced matrix in combination with benignly CNT carbon fiber surface coating techniques has shown to result in the deterioration of the composite's structural performance, thus failing to achieve multifunctionality.[40] In addition, CNT agglomeration and a greatly increased resin viscosity cause the complete dispersion of CNTs to be extremely difficult, therefore limiting the integration of such methods into industrial processes.[41]

Recently, zinc oxide (ZnO) nanowires (NWs) have been demonstrated to be a promising, multi-functional whiskerization material when vertically synthesized on the surface of reinforcing fibers. These fiber surfaces were whiskerized with arrays of ZnO NW through a hydrothermal (<90 °C) aqueous solution-based process, thus entirely preserving the strength of the fiber.[42–44] The piezoelectric nature of these NWs improve the fiber reinforced composites' functionality, allowing it to harvest energy from its surroundings and detect damage during operation.[6,45] Galan et al.[46] reported a 228% improvement in IFSS of carbon fiber reinforced polymers at quasi-static conditions, when the ZnO NWs with optimized aspect ratio were introduced onto the surface of the carbon fibers. It was reported that IFSS increased near-linearly with an increase in both the length and diameter of the NWs. Under static loading, the ZnO NWs provide out-of-plane reinforcement, creating a stiffness gradient between the dissimilar fiber and matrix materials, thus, reducing stress concentrations.[47] While there has been no research on the performance of a ZnO interphase in a carbon fiber reinforced composite at dynamic loading conditions, many studies have shown that a ZnO interphase can improve ballistic performance. Malakooti et al.[48] demonstrated that the addition of a ZnO NW interphase to hybrid carbon fiber composites leads to a remarkable increase in its damping properties and flexural rigidity. When ZnO NWs are added, a 200% increase in loss factor was observed, and the energy absorption of the composite was improved. Malakooti et al.[49] also reported a 66% increase in impact resistance of ZnO grown aramid fabrics with negligible increase in their weight. Elsewhere, Hwang et al.[50,51] reported an increase in interyarn friction of ZnO grown aramid fabric by 23 times induced by the increase

1901544 (2 of 11)

in surface area from the grafted interphase, allowing for a higher degree of interlocking between ZnO NWs and material buildup during tow pullout. The increase in interyarn friction when a ZnO interphase is added limits yarn mobility within the fabric and results in an improved ballistic performance. These studies have shown that a ZnO NW interphase can increase the IFSS of composites under static loading conditions, while showing great promise for being a suitable interphase in ballistic applications. Nonetheless, understanding the behavior of a ZnO interphase inside a fiber reinforced composite and its influence on the mechanical performance of the composites under intermediate and high strain rate loading conditions is important for its integration into ballistic applications. Yet as previously mentioned, this remains to be studied, characterized, or reported in the literature.

In this study, the IFSS of ZnO nanoparticle (NP) and NW-coated carbon fiber reinforced composites was characterized at intermediate and high strain rates and compared to that at quasi-static rates. Measurements of interfacial properties of fiber reinforced composites under dynamic loading conditions using single fiber IFSS testing was enabled using a recently developed experimental setup.[52] Vertically aligned ZnO NWs were uniformly synthesized on functionalized carbon fibers using a hydrothermal method before quantifying its effect on the IFSS, as well as the fiber's tensile strength, using appropriate mechanical testing and sample fabrication. Similar measurements were also conducted on untreated and ZnO NP-coated carbon fibers. The surface chemistry, morphology, and post pullout state of the modified carbon fibers were characterized using scanning electron microscopy (SEM) and X-ray photoelectron spectroscopy (XPS). The nanostructured interphase is found to strengthen the fiber–matrix interface under static loading, while weakening it under dynamic loading conditions, as the effect of the functional gradient is reduced. These results suggest that a ceramic ZnO NW interphase allows for the design of carbon fiber reinforced polymer matrix composites that simultaneously possess high structural and ballistic performance, demonstrating its potential as a novel multifunctional and lightweight ballistic protective material.

2. Results and Discussion

2.1. Synthesis and Characterization of ZnO Interphase

Surface morphology of carbon fibers following seeding and growth is characterized through SEM imaging. To accurately evaluate the mechanical performance of a ZnO interphase using pullout testing, it is important that the embedded lengths of tested fibers are sufficiently and uniformly coated with ZnO NPs and NWs. **Figure 1**A,B shows a side view of the roughened surface of the carbon fibers after NP deposition. The deposited NPs form a uniform, tightly packed thin film of which the bonding strength relies on the uniformity of the crystal sizes and structure. The dip-coated carbon fibers provide functional sites for the suspended ZnO NPs inside the ethanol solution to self-assemble on its surface. The diameters of these NPs were measured to vary between 10 and 15 nm and the thickness of the surface coating can be easily increased by performing

a larger number of dip-coating cycles. While the interfacial behavior of the ZnO NP interphase will be studied, it can also serve a seed layer for the radial growth of ZnO NWs on the fiber's surface (Figure 1C). As demonstrated by Lin et al.,[43] the seed layer nucleates into arrays of vertically aligned ceramic ZnO NWs on the surface of the carbon fibers when placed inside a growth solution. This observed NW geometry is attributed to the discrepancy of the growth rate between the [0001] polar face and the lateral faces.[53] Following growth, gentle washing of the fibers eliminates any ZnO crystalline prism precipitation deposited on the surface. This is a necessary step to ensure a defect-free and uniform fiber surface morphology, thus reducing errors and inaccuracies in IFSS measurements using pullout testing. As seen in Figure 1D, the dense ZnO NWs interphase uniformly covers the carbon fiber surface, providing a considerable increase in the surface area of carbon fibers and its capacity to mechanically interlock with the matrix. The interfacial reinforcing performance of the grown interphase is proven to be reliant on the morphology of the NWs, which can be tuned through a number of parameters such as growth period, addition of inhibitors.[46] The ZnO NWs used in this study were typically grown to possess an aspect ratio of 10, having a diameter of ≈100 nm and a length of ≈1 µm (Figure 1E–H). Previous studies reported an improvement in IFSS with increasing NW diameter and length under quasi-static loading conditions.[46] Finally, while the growth of the NWs is largely unaffected by the surface chemistry of the fiber, it should be noted that the adhesion and chemical interaction between the NWs and the fiber's surface heavily influences the performance of the interphase.

To achieve optimal performance under quasi-static loading, the adhesion between the grown NWs and the fiber surface is improved through functionalization. By further populating the carbon fiber surface with oxygen functional groups through oxidative methods, such as nitric acid oxidation, the ZnO interphase is expected to strongly adhere to the fiber surface.[44] Characterization of the nitric acid functionalization was performed using XPS, and the C 1s spectra for each sample are shown in **Figure 2**. The spectra show increasing oxygen functional groups after functionalization, and while the concentration of hydroxyl groups remains relatively unchanged, the concentration of ketones and carboxyl increase by 65% and 78%, respectively (**Table 1**). Unlike the lone pairs of hydroxyl and carboxyl functional groups, whose high steric hindrance limits any interaction with Zn ions, the high polarity of ketone groups' lone pairs of electrons strongly attracts the Zn ions in the crystal.[44] Therefore, the newly grafted oxygen groups enable strong binding between the ZnO NWs and the carbon fiber surface, which improves load transferring and mechanical interlocking between both constituents of the fiber–matrix interface.

2.2. Tensile Testing

To ensure a multifunctional, high ballistic, and structural performance, it is necessary that the tensile properties of carbon fiber remain intact. To confirm that the strength of carbon fibers is unaffected by the functionalization and interphase growth process, the tensile testing of treated fibers is performed
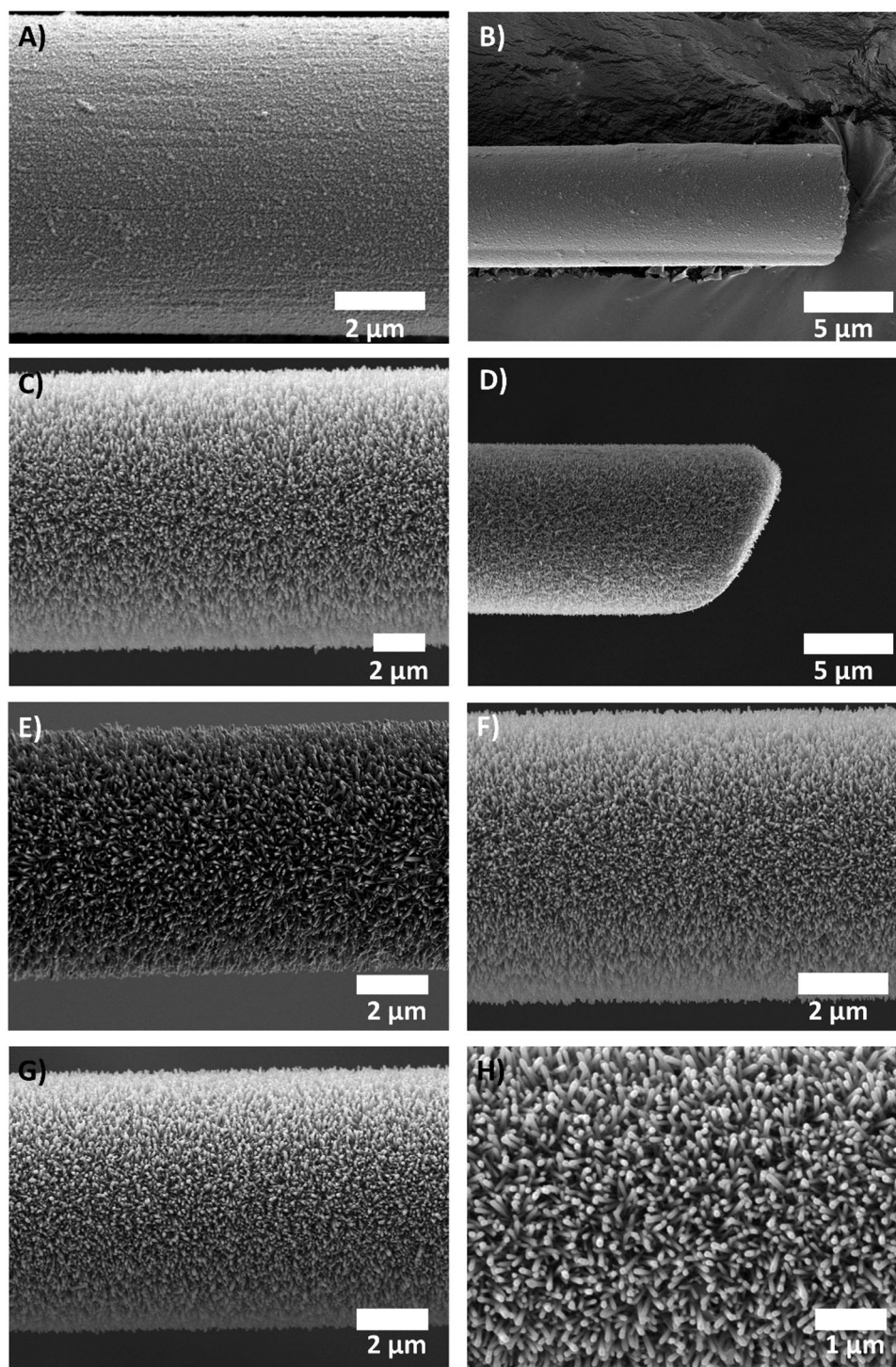
**ADVANCED
SCIENCE NEWS**

www.advancedsciencenews.com

**ADVANCED
MATERIALS
INTERFACES**

www.advmatinterfaces.de

Figure 1. Zinc oxide-coated carbon fibers. A,B) Zinc oxide NPs–coated carbon fibers. C–H) Zinc oxide NWs–coated carbon fibers.

following procedures described in ASTM C1557-03 standard at varying strain rates. The preservation of the carbon fiber's tensile strength is necessary for it to maintain its structural performance while also maximizing its ballistic speed limit. Hence, a suitable interphase and functionalization method should be able to retain the in-plane properties of composites, which is derived from the fibers' axial strength. Etching and surface

defects on the fiber are primary mechanisms by which the tensile strength of the fiber is reduced. While the strength of macroscale carbon fibers is typically limited by manufacturing defects, oxidative functionalization using chemical solutions can further amplify these limitations, therefore requiring a post-ZnO NWs growth re-assessment of the tensile strength of the fibers. Although tensile testing at quasi-static strain rates
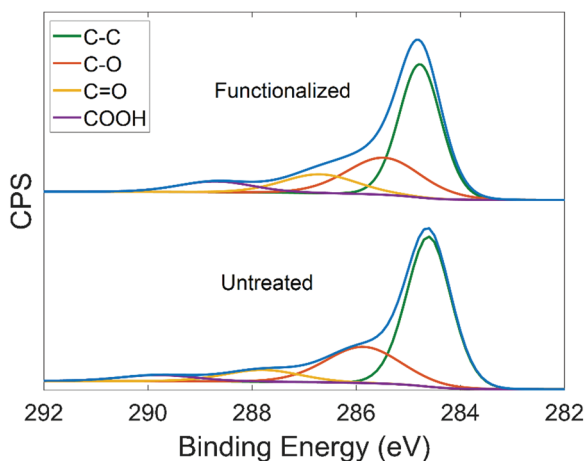
Figure 2. Deconvoluted and normalized C 1s XPS spectra of untreated and functionalized carbon fibers.

can be performed over numerous gauge lengths, the maximum possible gauge length at intermediate and high strain rates is restricted by the actuator's maximum displacement. Since the range of longitudinal deformation offered by the high strain rate piezoelectric stack is limited to 100 μm, and the strain to failure of carbon fibers at quasi-static loading is typically 1.7%, the maximum possible gauge length was found to be 5.88 mm. It should be noted that the strain to failure of carbon fibers can slightly decrease with increasing strain rate, resulting in a larger maximum gauge length. Ultimately, a gauge length of 3 mm was used across all testing strain rates to ensure consistency during comparison. After specimen fabrication, three sets of 15 fibers were axially loaded at quasi-static, intermediate, and high strain rate, respectively, and the ultimate tensile strength of the fibers was determined. According to **Figure 3**, at a quasi-static loading strain rate of 0.0016 s^{-1}, the tensile strength of ZnO NP-coated carbon fibers is statistically unchanged, while that of ZnO NWs-coated fiber increases by 10.2% in comparison to untreated fibers. Similar trends are also observed at intermediate and high strain rate tests of 470 and 2200 s^{-1}, respectively. The tensile strength of ZnO NW-coated carbon fibers is found to increase by 8.4% and 14.5% at 470 and 2200 s^{-1}, respectively, while that of ZnO NPs carbon fibers continues to remain unchanged. Such findings agree with reported tensile characteristics of various type of fibers when nanostructured whiskers are grafted on their surface.[49,50,54] A comparison of the tensile properties of fiber sets of similar surfaces across strain rates allows for further characterization of the ZnO interphase. The tensile strength of untreated, ZnO NP- and ZnO NW-coated fibers was found to be unaffected by the increase in strain rate. The insensitivity of carbon fiber to strain rate is an expected

Table 1. Decomposed C 1s energy state's concentrations and bonding-state peak locations of untreated and functionalized fibers.

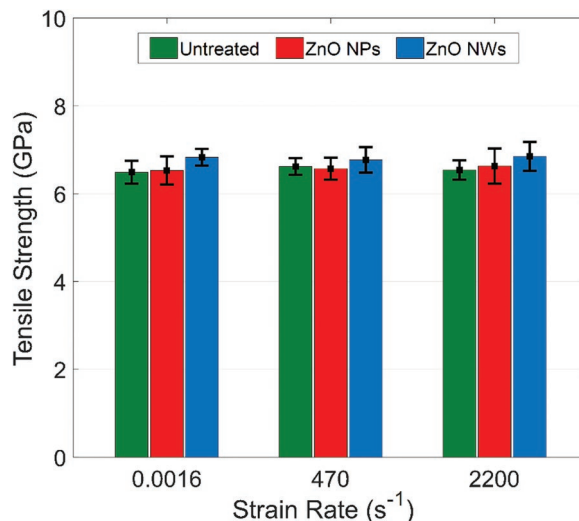| Carbon fiber	% C—C (284.7 eV)	% C—O (286.5 eV)	% C=O (287.8 eV)	% COOH (289.3 eV)
Untreated	62.24	25.32	8.2	4.24
Functionalized	53	26.2	13.25	7.55

Figure 3. Tensile strength of untreated and ZnO-coated fibers across various strain rates: 0.0016, 470, and 2200 s^{-1}.

phenomenon given its ceramic nature, as no viscoelastic effects are expected to affect its tensile behavior. Strain rate sensitivity is typically found in polymer fibers, such as aramids, where the quasi-static tensile loading evokes the viscous and damping properties of the fibers, while higher strain rates are dominated by the fiber's elastic properties.[55] It can be concluded that the tensile strength of the carbon fibers is fully preserved after functionalization and the addition of the ZnO interphase, and that it is independent of the applied strain rate, indicating that in-plane properties of carbon fiber reinforced composites are not at risk of decreasing.

2.3. Interfacial Properties and Strain Rate Dependency

While maintaining the in-plane properties of a fiber reinforced composite is necessary, the ability of the composite to achieve its theoretical properties heavily relies on the quality and design of its fiber–matrix interface and the interaction between both of its components. When quasi-statically loaded, a well bonded and adhered fiber–matrix interface contributes to a reinforcement effect inside the composite, as it bridges the discontinuities found in such heterogenous materials and allows for an improved load transfer from the compliant matrix to the tough fibers. However, a different fiber–matrix behavior is required under dynamic loading conditions. At high loading rates, the composite interface is typically designed with weak adhesion such that the tough fibers separate from the matrix, allowing them to absorb the impact. As the fiber releases from the matrix, there is significant energy absorption due to the friction between both components. Such different fiber–matrix properties can be simultaneously satisfied by the grafting of a ZnO interphase on the surface of carbon fibers. To prove this, the IFSS of the interface between coated fiber and epoxy matrix was quantified using single fiber pullout testing (SFP) at low, intermediate, and high strain rate loading conditions. The SFP at intermediate and high strain rates was performed using the experimental setup described first by Hwang et al.[52]
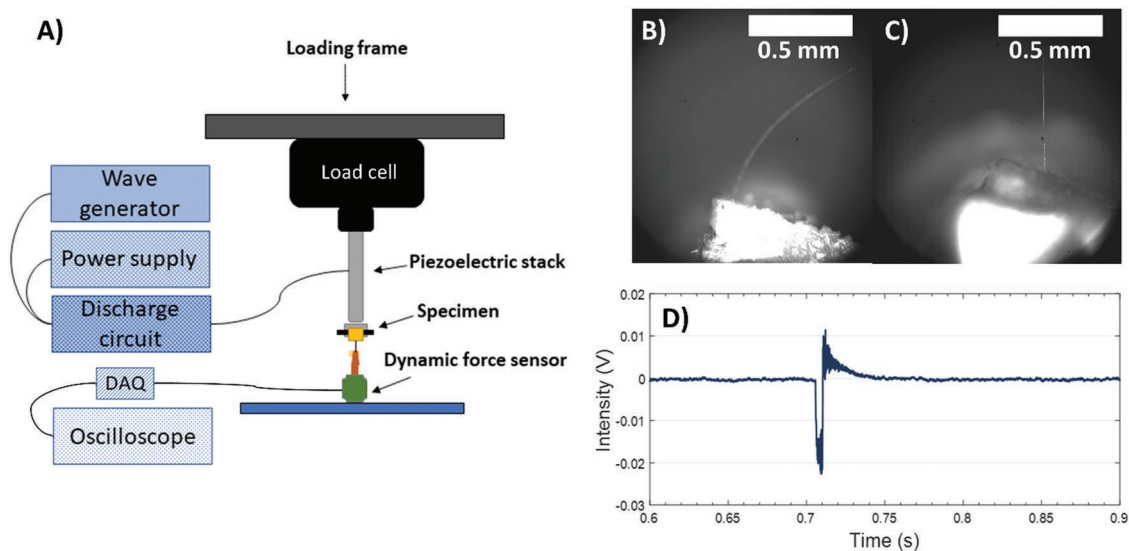
Figure 4. A) Schematic of experimental setup for intermediate and high strain rate single fiber pullout testing. B,C) High speed camera image of the initial fiber position and vertically aligned and re-strained carbon fiber ready for testing. D) Dynamic load cell–recorded voltage–time response of the pullout process.

The experimental procedure, seen in **Figure 4**A, uses a piezoelectric actuator coupled with a discharge circuit that allows up to 10^4 s^{-1} in strain rate and 100 µm in displacement. While the experimental setup is capable of simulating a wide range of strain rates, strain rates of 470 and 2200 s^{-1} were used to dynamically load the fiber–matrix interface. The selected strain rates mimic typical intermediate and high strain rates dynamic conditions to which composites used in ballistic applications are usually subjected. Moreover, these strain rates are several orders of magnitude larger than that used for quasi-static loading of 0.0016 s^{-1}, thus accurately replicating dynamic conditions relative to quasi-static IFSS testing. The embedded lengths of the specimens were designed to be smaller than 60 µm using an optical microscope, so that it satisfies the displacement limitations of the actuator. The design of the molds ensures that the embedded lengths of specimens remain unchanged post-curing, as the fiber is immobilized inside the molds' slits. This is further confirmed by examination of the specimens' embedded lengths before testing. When choosing the embedded fiber length for SFP testing, it is mandatory for it to satisfy multiple distinct criteria. First, it should ensure that interfacial failure happens before tensile failure by accounting for the maximum applied pullout load. Second, the embedded fiber length should result in a catastrophic failure of the interface, and therefore a linear elastic stress–strain behavior throughout the pullout test. This is primarily important in order to avoid initiating interfacial failure through crack propagation, thus leading to inaccurate IFSS calculation due to effect of frictional forces.[56] As discussed later, this is also necessary to maintain consistency in testing procedures for both static and dynamic loading conditions, as the piezoelectric actuator may be unable to ensure complete fiber pullout, while the dynamic load cell is incapable of accurately recording the frictional effects. Finally, the embedded length is designed to be considerably larger than the fiber's diameter in order to satisfy the assumption of a cylindrical embedded fiber geometry

and avoid cross-sectional effects. Added to that, choosing an embedded length that is less than 60 µm eliminates any considerations with regards to Poisson shrinkage effects.[57] The fiber's free length is another parameter that requires proper design to ensure successful pullout across all strain rates since the free length will strain, and if not accounted for can absorb the 100 µm stack displacement. For a clean fiber pullout from the matrix, the fiber's free length is required to store sufficient energy to ensure the embedded length's pullout. Meanwhile, the elastic deformation of the fiber's free length should also be chosen to be smaller than the fiber's embedded length, a feature that is proportionally dependent on the fiber's free length.[57] The proximity of the embedded lengths to the actuator's maximum displacement requires for a perfect vertical alignment at the start of the test, which was maintained using a high-speed camera (Figure 4B,C) and the application of a minimal pre-load of ≈0.0178 N to the fiber. The pre-load of the fiber was kept consistent across all samples, as it was controlled using the fine precision controller of the testing frame and monitored through a static load cell. Once discharge is initiated, the IFSS is calculated using the voltage–time response recorded through a piezoelectric shock load cell (Figure 4D). Unlike the load–displacement curves generated under quasi-static loading, here, the pullout process results in an instantaneous voltage signal inside the piezoelectric dynamic load cell whose period is dependent on the applied strain rate. The trailing oscillations caused by post-pullout vibrations of the grip are transient and can be isolated from the detected pullout load signal that precedes it. Using such load measurement technique, frictional effects during pullout are difficult to accurately capture, further justifying the adopted design approach for SFP specimens. The discharge time is inversely proportional to the applied strain rate and is represented through the duration of the response. Finally, the piezoelectric actuator's displacement is kept at 90 µm for all tested specimens.

**ADVANCED
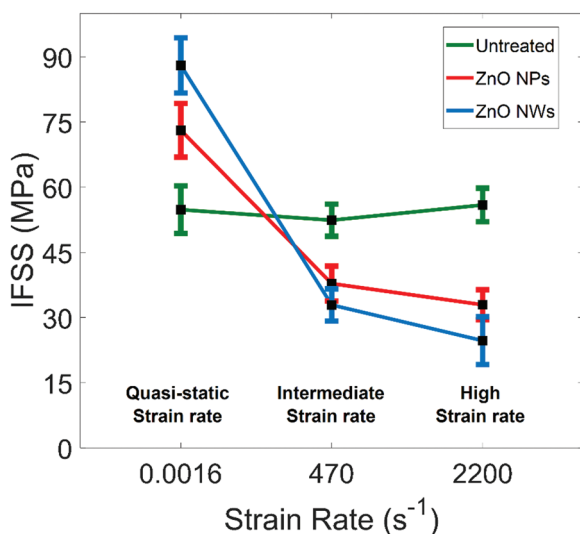SCIENCE NEWS**

www.advancedsciencenews.com

**ADVANCED
MATERIALS
INTERFACES**

www.advmatinterfaces.de

Figure 5. Interfacial shear strength of untreated and ZnO-coated fibers across various strain rates: 0.0016, 470, and 2200 s^{-1}.

Irrespective of the applied loading rate, the IFSS of untreated carbon fibers shows no significant statistical change, remaining relatively constant at approximately 49 MPa (**Figure 5**). The observed rate independency in the IFSS of the untreated single carbon fiber composites is expected given the ceramic nature of the loaded fibers. Given that carbon fibers exhibit no stiffening effect with increasing strain rate, interfacial properties are solely expected to be dependent on the fiber–matrix interaction. In untreated and functionalized carbon fibers, the quality of the fiber–matrix interface is dictated by two rate-independent parameters: the chemical interaction and mechanical interlocking between both components. Moreover, by designing pullout testing for catastrophic interfacial failure, frictional and additional shearing effects between the fiber and the matrix are eliminated. Elsewhere, the IFSS of ZnO NW- and NP-coated carbon fibers is found to be dependent on loading conditions. At a quasi-static loading rate of 0.0016 s^{-1}, a maximum IFSS of 85.6 MPa is observed for ZnO NW-coated fibers, showing approximately an 87% increase from an IFSS of 48.7 MPa for the untreated fibers. However, as loading rate is increased to 470 and 2200 s^{-1}, the IFSS of ZnO NW-coated fibers is decreased to 32 and 23 MPa, respectively. Similarly, when compared to untreated carbon fibers, ZnO NP-coated fibers display a 35% increase in IFSS when quasi-statically loaded, and a 20% and 38% decrease in IFSS when loaded at intermediate and high strain rates, respectively. IFSS of the ZnO-coated fibers thus displays a decreasing trend with increasing strain rate, with either higher or lower IFSS than that of untreated carbon fibers under identical loading conditions. Moreover, Figure 5 shows that a ZnO NW interphase transitions from a higher IFSS relative to that of a ZnO NP interphase at a quasi-static loading rate, to a lower one at intermediate and high strain rates, as the IFSS of ZnO NW-coated fibers goes from being 21% higher IFSS than ZnO NP-coated fibers at 0.0016 s^{-1}, to 17% and 25% lower IFSS at 470 and 2200 s^{-1}, respectively. This indicates the influence of the interphase's geometry, especially its aspect ratio, on its performance across strain rates,

causing NWs and NPs to exhibit different failure modes when the fiber–matrix interface is dynamically loaded. The observed decrease in IFSS is a result of the weaker fiber–matrix interface, a desirable interfacial property for dynamic loading conditions. Such results offer insight into the reversing of the role of a ZnO interphase inside a composite when loading rate is increased. At a quasi-static loading rate, the rigid ceramic NWs penetrate into the matrix, providing localized reinforcement by increasing the bonding area and improving load transfer. The functionally graded interface bridges the typically discrete boundaries of the fiber–matrix interface, reducing stress concentrations and improving the IFSS of the composite. However, the observed decrease in IFSS of ZnO NP- and NW-coated carbon fibers with increasing strain rates demonstrates the ability of a ZnO interphase to allow easier interfacial debonding under dynamic loading conditions. Therefore, the effectiveness of the functional grading provided by the ZnO interphase is decreased at intermediate and high strain rates, as the fiber–matrix interface exhibits premature failure.

The rate dependency of the IFSS in the presence of a ZnO interphase can be further explained by examining the polymer matrix's behavior as strain rate is increased. The EPON 862 polymer matrix used during pullout testing is expected to display a rate-dependent viscoelastic behavior. Stiffness measurements of the EPON 862 matrix were performed using the same setup described for static and dynamic pullout and tensile testing. At a strain rate of 2200 s^{-1}, a matrix elastic modulus of 9.2 GPa is observed, showing approximately a 187.5% increase from an elastic modulus of 3.24 GPa at 0.0016 s^{-1} (**Figure 6**). Such measurements are in agreement with other studies reported in literature discussing the viscoelastic behavior of polymers across strain rates.[58,59] This considerable increase in matrix stiffness changes the load transfer mechanism between the fiber and the matrix due to a ZnO interphase. Malakooti et al.[47] experimentally studied the effect of a whiskerized interphase on strain distribution at the interface region. They reported that the higher stiffness of the nanocomposite interphase leads to a reduction of shear strain and pushes it to the softer matrix. Based on the shear lag theory, the shear stress at the matrix would be lower due to its greater distance from the fiber in the presence of the
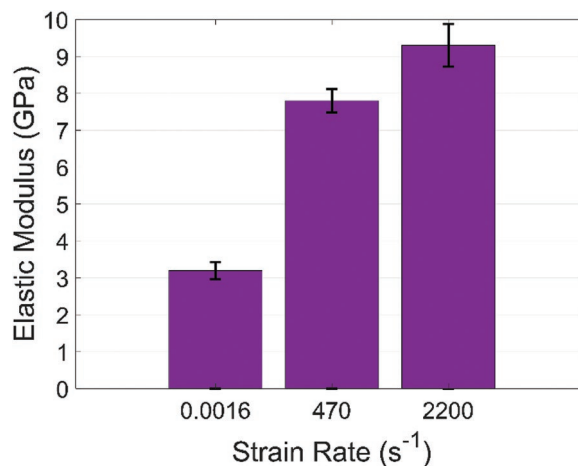

Figure 6. Elastic modulus of neat EPON 862 epoxy across various strain rates: 0.0016, 470, and 2200 s^{-1}.

1901544 (7 of 11)

**ADVANCED
SCIENCE NEWS**
www.advancedsciencenews.com

**ADVANCED
MATERIALS
INTERFACES**
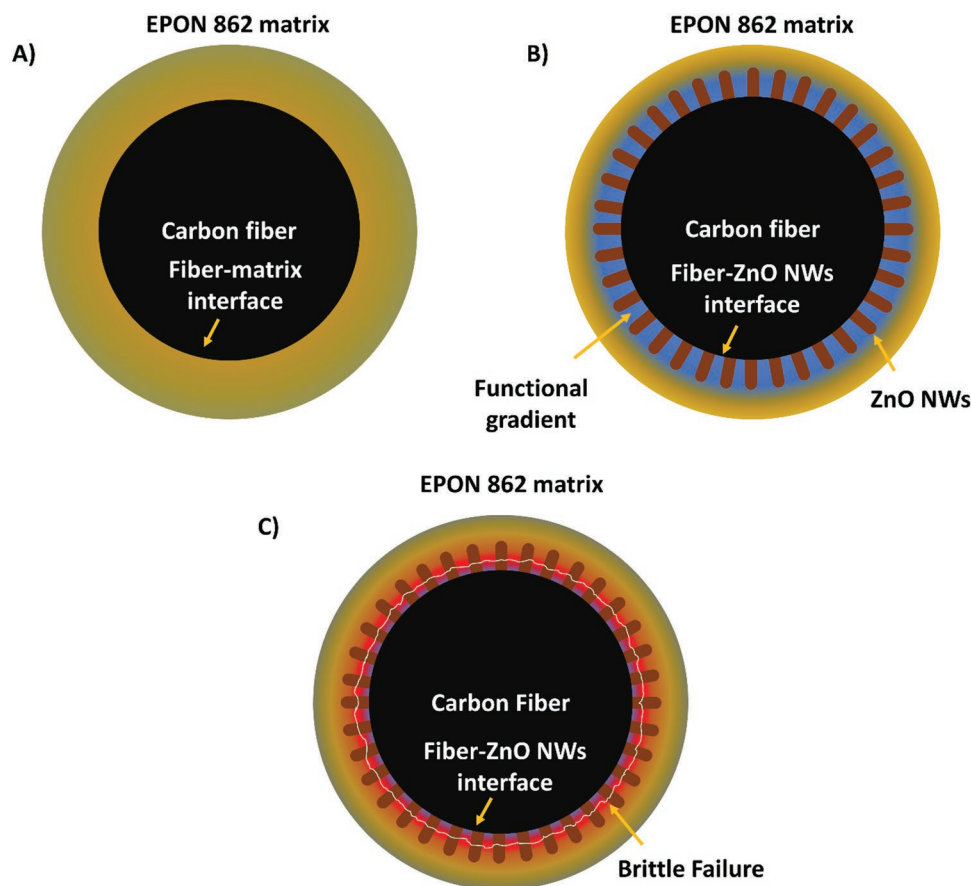www.advmatinterfaces.de

Figure 7. Failure mechanism of ZnO interphase under varying loading rates. A) Traditional carbon fiber–matrix interface subjected to shear strain. B) Functional gradient effect of a ZnO interphase under static loading conditions, smoothening interfacial shear strain transition, and reducing stress concentrations (blue region). C) Brittle failure of the ZnO interphase under dynamic loading conditions due to stiffening of matrix and interphase.

NWs.[60] In addition, the NWs create a functional gradient that smoothens the transition of shear strains between the elastically mismatched interfacial constituents (**Figure 7**B). The following eliminates local strain concentrations in the vicinity of the fiber interfacial region and moves it away a considerable distance, and into the relatively tougher and more crack-resistive epoxy matrix (Figure 7A). Such findings also explain how a nanostructured gradient can result in large interfacial shear strengths that exceed that of the matrix,[61] thus avoiding matrix shear failure before interfacial debonding. Under such conditions, fiber pullout occurs when the ZnO NWs/carbon fiber interface fails which is dependent on the chemical interaction between the ZnO interphase and the fiber surface. However, as loading conditions are changed and strain rate is increased, the matrix surrounding the interphase stiffens, thus weakening its functional gradient and re-introducing interfacial shear strain concentrations. This results in an unusual and sudden shear loading of the ZnO interphase which would cause brittle failure (Figure 7C). Moreover, ZnO NWs and NPs are ceramic nanomaterials of wurtzite structure, that when loaded at room temperatures, tend to fail in a brittle manner along the (0001) cleavage plane.[62–64] Under dynamic loading, these ceramics also display an increase in stiffness and a decrease in ductility, reducing its strain to failure. With that, the interfacial failure mode is

modified, as the ZnO interphase experiences brittle failure before debonding from the fiber surface, leading to disconnections in the functionally graded interface and allowing for easier debonding between the fiber and the matrix.

Further insight into the interfacial failure mechanism is obtained through examination of the embedded portion of the carbon fiber post-testing using SEM imaging. The embedded section of quasi-statically loaded ZnO NW-coated carbon fibers is shown in **Figure 8**A–C, which displays clean, NWs-free surfaces. The ZnO NWs are initially strongly bonded to the carbon fiber surface through ketone functional groups, as well to the matrix through an embedded, stiff, and large bonding area, providing two interfaces that are stronger than the traditional carbon fiber-epoxy interface.[43] Under quasi-static loading, the ZnO NWs detach from the surface of the carbon fibers and remain interlocked inside the matrix. This is due to the interaction area between the matrix-NWs interface being considerably larger than that of the fiber surface–NW interface, resulting in the initiation of interfacial failure at the level of the latter. Moreover, the absence of any resin residue on the fiber surface indicates that the matrix does not exhibit failure in the presence of a ZnO interphase, even at high IFSS of 90 MPa. In comparison, the surface of untreated embedded carbon fiber lengths is also found to be relatively smooth due to the brittle nature
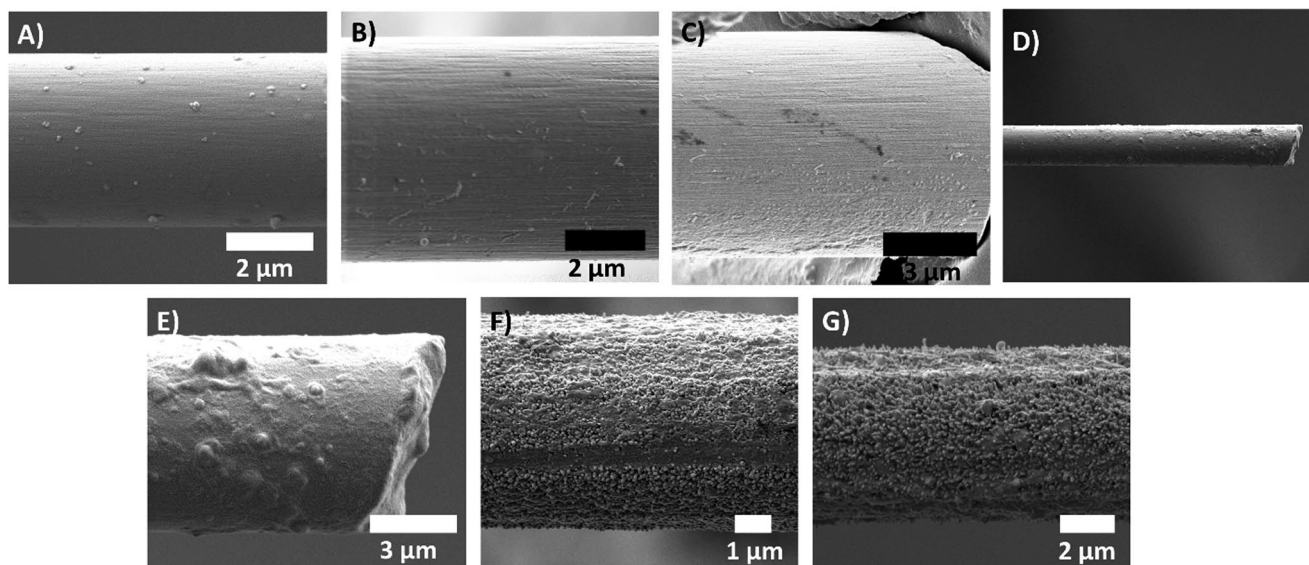
Figure 8. A,B) SEM images of the embedded length following pullout of: A–C) ZnO NWs–coated carbon fibers at quasi-static loading rate. D,E) Untreated carbon fibers at quasi-static loading rate. F,G) ZnO NWs–coated carbon fibers at 2200 s⁻¹.

of EPON 862 (Figure 8D,E). However, unlike the case of ZnO NWs-coated fibers, the surface of untreated fibers still displays residual matrix material in a number of spots. The interfacial shear testing methodology used in this work does not allow for examining the ZnO NWs–epoxy interface, nor the matrix itself, yet the observed ZnO NWs-free embedded lengths surfaces confirm the NWs remain anchored inside the matrix. Under dynamic loading of 2200 s⁻¹, the interfacial failure mode is changed, as the debonding of the ZnO interphase is preceded by a brittle failure of the ZnO interphase, as the surrounding matrix stiffens. Figure 8F,G shows bundles of broken ZnO NWs that remain attached to the carbon fiber surface post-pullout. However, it is difficult to assess these fractured NWs, as the surrounding and embedding matrix impedes proper assessment of their lengths. These SEM images support the failure mechanism in Figure 7C, as the ZnO interphase is expected to fail before complete debonding of the NWs from the fibers' surface. The resulting brittle failure of the ZnO interphase reduces the IFSS of the single fiber composites specimens with increasing loading rate up to where a ZnO interphase is weaker than a traditional carbon fiber–matrix interface. With that, easier debonding of the fibers from the matrix is achieved, allowing them to carry the load in the cases of impact or ballistic events. Finally, it should be noted that the geometry and aspect ratio of the ZnO interphase plays an important role during failure. The vertically aligned NWs are firmly embedded inside the epoxy matrix, whereas the spherical ZnO NPs roughen the carbon fiber surface. Therefore, ZnO NWs offer a higher degree of mechanical interlocking and superior reinforcement performance under quasi-static loading. However, when dynamically loaded, the embedded NWs are highly constrained when epoxy matrix stiffens, increasing the possibility of brittle interphase failure, and leading to a lower IFSS through a ZnO NWs interphase in comparison with that of a ZnO NPs interphase. It can be then concluded that under dynamic loading conditions, brittle failure of the ZnO interphase, especially NWs, allows for

easier release of the fibers from the matrix, and an improved performance of carbon fiber reinforced composites in ballistics and impact applications, while maintaining its reinforcement role in quasi-static loading applications through the introduction of a functionally graded interface.

3. Conclusions

This paper has displayed the ability to tailor the interfacial properties of fiber reinforced composites for the design of multifunctional materials that behave optimally under both static and dynamic loading conditions. Zinc oxide NPs and NWs interphases are introduced on the surface of nitric acid-functionalized carbon fibers to improve its interfacial shear strength under quasi-static loading conditions through a combination of mechanical interlocking and increased surface area. Under dynamic loading conditions, brittle failure of the ZnO interphases reduces the IFSS of carbon fiber reinforced composites, allowing for an enhanced ballistic performance. The ZnO NPs-coated carbon fibers displayed an overall 40% and 58% decrease in IFSS at intermediate and high loading strain rates of 470 and 2200 s⁻¹, respectively. Similarly, ZnO NW-coated carbon fibers exhibited 62% and 73% decrease in IFSS at similar loading rates. The reduced IFSS under dynamic loading conditions is due to the stiffening of the polymer matrix at higher strain rates, limiting the effectiveness of the interphase's functional gradient, and leading to its brittle failure. Such a unique interfacial performance allows for the tough fibers to absorb the ballistic impact energy in the event of dynamic loading, while preserving its structural properties. Thus, ZnO interphases enable the design of multifunctional carbon fiber reinforced composites, with optimal performance under both static and dynamic loading conditions, giving way toward the integration of light-weight and flexible ballistic protection into structural components.
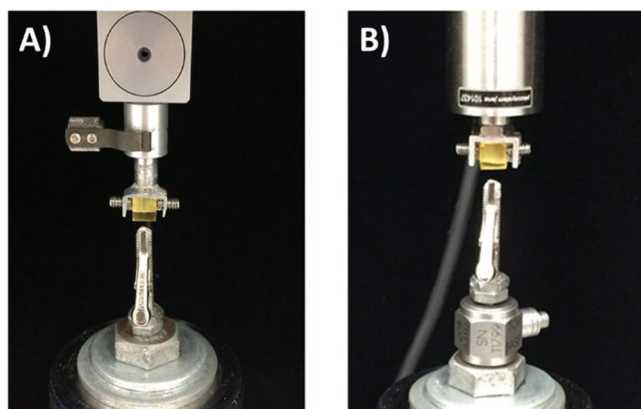
**ADVANCED
SCIENCE NEWS**

www.advancedsciencenews.com

**ADVANCED
MATERIALS
INTERFACES**

www.advmatinterfaces.de

Figure 9. Single fiber pullout experimental setup at: A) quasi-static strain rate. B) Intermediate and high strain rate.

4. Experimental Section

Fiber Functionalization, ZnO NWs Growth, and Characterization: AS-4 carbon fibers (Hexcel) were sonicated in acetone and ethanol successively, and functionalized through an oxidative technique in order to increase the oxygen surface functional groups.[44] Nitric acid oxidation was performed through first refluxing AS-4 carbon fiber tows in 100 mL of 70% nitric acid (70%, ACS certified: Fisher Scientific) for 4 h. Soxhlet extraction was then performed for 8 h in order to wash the fibers with deionized water, before further ultra-sonication for 15 min and drying at 100 °C overnight.

A ZnO NPs seeding solution was prepared using a multiple steps synthesis process. First, a 0.02 M solution of sodium hydroxide (NaOH) (ACS certified: Fisher Scientific) in ethanol and a 0.0125 M solution of zinc acetate dihydrate ($Zn(CH_3CO_2)_2 \cdot 2H_2O$) (Alfa Aesar) in ethanol were prepared and vigorously stirred at 60 and 50 °C, respectively. Once both solutions were dissolved completely, 32 mL of the sodium hydroxide solution was diluted in 80 mL of ethanol, while 32 mL of the zinc acetate solution was diluted in 256 mL of ethanol and both the solutions were heated up to 55 °C. The sodium hydroxide solution was added dropwise to the zinc acetate solution, then the solution was vigorously stirred for 45 min in a sealed glass jar to yield 516 mL of seeding suspension. Finally, the suspension was quenched in an ice bath to interrupt the growth of the ZnO NPs. In order to grow zinc oxide NWs on the fiber's surface, individual carbon fibers were laid across nylon frames and successively sonicated in acetone and ethanol for 10 min. Once clean, the frames were dipped in the seeding solution to deposit ZnO NPs on the fiber's surface, before annealing them in a convection oven for 10 min at 150 °C. The same process was repeated two more times, while allowing for a cooling down period of 5 min between cycles. The frame was placed inside an aqueous growth solution of equal molar concentrations of hexamethylenetetramine ($C_6H_{12}N_4$) (Alfa Aesar) and zinc nitrate hexahydrate ($Zn(NO_3)_2 \cdot 6H_2O$) (Alfa Aesar) at 150 °C s for 150 min. After removal from the growth solution, ultrapure water and methanol washings were performed on the ZnO NW-coated fibers, respectively, and the fibers were dried at 100 °C overnight. It should be noted that ZnO NP-coated carbon fibers were prepared using a similar seeding process, while omitting the final growth process. Prior to testing, SEM imaging was performed on a JEOL 7800 FLV to ensure a uniform coating on the fibers. XPS was also used to characterize the surface chemistry of untreated and functionalized carbon fibers. The data were collected using a Kratos Axis Ultra XPS and processed on a CASA-XPS software. The high-resolution spectrum was fit and decomposed into oxidative states components through a Marquette regression function, where each set of data set was fit with curves that were constrained in location and full-width at half-maximum of 1.1–1.7 eV.

Mechanical Testing: The interfacial shear strength of ZnO NW- and ZnO NP-coated carbon fibers inside epoxy matrix at varying strain rates

was measured using single-fiber pullout testing. After ZnO NW growth, the coated carbon fibers were embedded inside the slit of silicone molds that were coated with release agent. The embedded lengths were ensured to be less than 100 μm using an optical microscope. The matrix was consisted of resin blend of EPON 862 and Curing Agent W (Momentive Inc.) with a mixing ratio of 100:26.4 that was poured into the molds and cured at 121 °C for 6 h. Once curing was complete, 5 min epoxy (Loctite) tabs were placed at the fiber's free end for testing. IFSS was measured using single-fiber pullout testing at a quasi-static strain rate of 16 μm s^{-1} on a 5982 series Instron load frame (**Figure 9**A). The success of the pullout process was inspected using an optical microscope examination that ensured complete fiber pullout from the epoxy block. For dynamic loading, single fiber pullout was performed using the experimental setup described in Hwang et al.[52] at intermediate and high strain rates of 470 and 2200 s^{-1}, respectively (Figure 9B). Tensile tests of ZnO NWs-coated carbon fibers were also performed. Cardboard frames with gauge length of 3 mm, along with 5 min epoxy, were used in order to fix the fibers. The tensile strength of carbon fibers at low strain rate was evaluated at an extension rate of 16 μm s^{-1} on the load frame using a 5 N static load cell. The tensile strength of the fibers was measured at intermediate and high strain rates of 470 and 2200 s^{-1}, respectively, using the same setup described for dynamic pullout testing. Following pullout testing at all strain rates, the embedded lengths of the ZnO NWs-coated fibers were inspected using SEM imaging to elucidate the failure mechanism.

Conflict of Interest

The authors declare no conflict of interest.

[1] L. Zhang, X. Tian, M. H. Malakooti, H. A. Sodano, *Compos. Sci. Technol.* **2018**, *168*, 96.

[2] R. Das, C. Melchior, K. M. Karumbaiah, in *Adv. Compos. Mater. Aerosp. Eng.*, Elsevier **2016**, pp. 333–364.

[3] K. Marshiya, W. Zhang, *Composites, Part A* **2007**, *38*, 1116.

[4] S. Hayes, W. Zhang, M. Branthwaite, F. Jones, *J. R. Soc., Interface* **2007**, *4*, 381.

[5] Y. Yang, L. Tang, H. Li, *Smart Mater. Struct.* **2009**, *18*, 115025.

[6] M. H. Malakooti, B. A. Patterson, H.-S. Hwang, H. A. Sodano, *Energy Environ. Sci.* **2016**, *9*, 634.

[7] M. Aureli, C. Prince, M. Porfiri, S. D. Peterson, *Smart Mater. Struct.* **2010**, *19*, 015003.

[8] J. Nunes-Pereira, V. Sencadas, V. Correia, J. G. Rocha, S. Lanceros-Méndez, *Sens. Actuators, A* **2013**, *196*, 55.

[9] C. Li, E. T. Thostenson, T.-W. Chou, *Compos. Sci. Technol.* **2008**, *68*, 1227.

**ADVANCED
SCIENCE NEWS**

www.advancedsciencenews.com

**ADVANCED
MATERIALS
INTERFACES**

www.advmatinterfaces.de

[10] H.-K. Kang, D.-H. Kang, H.-J. Bang, C.-S. Hong, C.-G. Kim, *Smart Mater. Struct.* **2002**, *11*, 279.

[11] S. Wang, D. D. L. Chung, *Carbon* **2006**, *44*, 2739.

[12] I. Kang, M. J. Schulz, J. H. Kim, V. Shanov, D. Shi, *Smart Mater. Struct.* **2006**, *15*, 737.

[13] Y. Zou, L. Tong, G. P. Steven, *J. Sound Vib.* **2000**, *230*, 357.

[14] K. Diamanti, C. Soutis, *Prog. Aeronaut. Sci.* **2010**, *46*, 342.

[15] W. J. Staszewski, S. Mahzan, R. Traynor, *Compos. Sci. Technol.* **2009**, *69*, 1678.

[16] A. Bhatnagar, *Lightweight Ballistic Composites*, Elsevier, New York **2016**.

[17] V. P. McConnell, *Reinf. Plast.* **2006**, *50*, 20.

[18] B. K. Fink, *J. Thermoplast. Compos. Mater.* **2000**, *13*, 417.

[19] R. A. Mcgrane, *M.Sc. Thesis*, Virginia Polytechnic Institute and State University, **2001**.

[20] A. C. Morgan, *US20110203024A1*, **2010**.

[21] L. B. Tan, K. M. Tse, H. P. Lee, V. B. C. Tan, S. P. Lim, *Int. J. Impact Eng.* **2012**, *50*, 99.

[22] R. G. Norris, *US7797764B2*, **2005**.

[23] D. J. Harach, K. S. Vecchio, *Metall. Mater. Trans. A* **2001**, *32*, 1493.

[24] K. S. Vecchio, *JOM* **2005**, *57*, 25.

[25] B. Vieille, V. M. Casado, C. Bouvet, presented at 15th European Conf. Composite Materials, Venice, Italy, June **2012**.

[26] M. Tanoglu, S. McKnight, G. Palmese, J. Gillespie Jr, *Compos. Sci. Technol.* **2001**, *61*, 205.

[27] M. M. Ansari, A. Chakrabarti, *Procedia Eng.* **2017**, *173*, 161.

[28] W. Goldsmith, C. K. H. Dharan, H. Chang, *Int. J. Solids Struct.* **1995**, *32*, 89.

[29] K. K. Chawla, *Composites* **1989**, *20*, 286.

[30] B. L. Lee, T. F. Walsh, S. T. Won, H. M. Patts, J. W. Song, A. H. Mayer, *J. Compos. Mater.* **2001**, *35*, 1605.

[31] R. L. Gorowara, W. E. Kosik, S. H. McKnight, R. L. McCullough, *Composites, Part A* **2001**, *32*, 323.

[32] Z. Dai, F. Shi, B. Zhang, M. Li, Z. Zhang, *Appl. Surf. Sci.* **2011**, *257*, 6980.

[33] J.-K. Kim, Y. W. Mai, *Engineered Interfaces in Fiber Reinforced Composites* (Eds: J.-K. Kim, Y.-W. Mai), Elsevier Sciences, New York **1998**.

[34] B. Gao, R. Zhang, F. Gao, M. He, C. Wang, L. Liu, L. Zhao, H. Cui, *Langmuir* **2016**, *32*, 8339.

[35] S. P. Sharma, S. C. Lakkad, *Composites, Part A* **2015**, *69*, 124.

[36] C. Fernández, C. Medina, G. Pincheira, C. Canales, P. Flores, *Composites, Part B* **2013**, *55*, 421.

[37] M. Tehrani, A. Y. Boroujeni, T. B. Hartman, T. P. Haugh, S. W. Case, M. S. Al-Haik, *Compos. Sci. Technol.* **2013**, *75*, 42.

[38] E. Bekyarova, E. T. Thostenson, A. Yu, H. Kim, J. Gao, J. Tang, H. T. Hahn, T.-W. Chou, M. E. Itkis, R. C. Haddon, *Langmuir* **2007**, *23*, 3970.

[39] W. B. Downs, R. T. K. Bakera, *J. Mater. Res.* **1995**, *10*, 625.

[40] A. Godara, L. Gorbatikh, G. Kalinka, A. Warrier, O. Rochez, L. Mezzo, F. Luizi, A. W. van Vuure, S. V. Lomov, I. Verpoest, *Compos. Sci. Technol.* **2010**, *70*, 1346.

[41] J. Gibson, J. McKee, G. Freihofer, S. Raghavan, J. Gou, *Int. J. Smart Nano Mater.* **2013**, *4*, 212.

[42] G. J. Ehlert, H. A. Sodano, *ACS Appl. Mater. Interfaces* **2009**, *1*, 1827.

[43] Y. Lin, G. Ehlert, H. A. Sodano, *Adv. Funct. Mater.* **2009**, *19*, 2654.

[44] G. J. Ehlert, U. Galan, H. A. Sodano, *ACS Appl. Mater. Interfaces* **2013**, *5*, 635.

[45] L. Groo, D. J. Inman, H. A. Sodano, *Adv. Funct. Mater.* **2018**, *28*, 1802846.

[46] U. Galan, Y. Lin, G. J. Ehlert, H. A. Sodano, *Compos. Sci. Technol.* **2011**, *71*, 946.

[47] M. H. Malakooti, Z. Zhou, J. H. Spears, T. J. Shankwitz, H. A. Sodano, *Adv. Mater. Interfaces* **2016**, *3*, 1500404.

[48] M. H. Malakooti, H.-S. Hwang, H. A. Sodano, *ACS Appl. Mater. Interfaces* **2015**, *7*, 332.

[49] M. H. Malakooti, H.-S. Hwang, N. C. Goulbourne, H. A. Sodano, *Composites, Part B* **2017**, *127*, 222.

[50] H.-S. Hwang, M. H. Malakooti, H. A. Sodano, *Composites, Part A* **2015**, *76*, 326.

[51] H.-S. Hwang, M. H. Malakooti, B. A. Patterson, H. A. Sodano, *Compos. Sci. Technol.* **2015**, *107*, 75.

[52] H. S. Hwang, J. Nasser, H. A. Sodano, *Exp. Mech.* **2019**, *59*, 979.

[53] G. J. Ehlert, *Ph.D. Thesis*, University of Florida, **2012**.

[54] E. D. LaBarre, X. Calderon-Colon, M. Morris, J. Tiffany, E. Wetzel, A. Merkle, M. Trexler, *J. Mater. Sci.* **2015**, *50*, 5431.

[55] I. P. Giannopoulos, C. J. Burgoyne, presented at 16th National Conf. Concrete Structure, Paphos Cyprus, October **2009**.

[56] P. J. Herrera-Franco, L. T. Drzal, *Composites* **1992**, *23*, 2.

[57] P. S. Chua, M. R. Piggott, *Compos. Sci. Technol.* **1985**, *22*, 33.

[58] A. Gilat, R. K. Goldberg, G. D. Roberts, *J. Aerosp. Eng.* **2007**, *20*, 75.

[59] C. R. Siviour, J. L. Jordan, *J. Dyn. Behav. Mater.* **2016**, *2*, 15.

[60] T. W. Clyne, *Mater. Sci. Eng., A* **1989**, *122*, 183.

[61] D. R. Klimek-McDonald, J. A. King, I. Miskioglu, E. J. Pineda, G. M. Odegard, *Polym. Compos.* **2018**, *39*, 1845.

[62] R. Agrawal, B. Peng, H. D. Espinosa, *Nano Lett.* **2009**, *9*, 4177.

[63] A. V. Desai, M. A. Haque, *Sens. Actuators, A* **2007**, *134*, 169.

[64] S. Hoffmann, F. Östlund, J. Michler, H. J. Fan, M. Zacharias, S. H. Christiansen, C. Ballif, *Nanotechnology* **2007**, *18*, 205503.